

Quantum Nature in the Interaction of Molecular Hydrogen with Porous Materials: Implications for Practical Hydrogen Storage

Srimanta Pakhira* and Jose L. Mendoza-Cortes*

Cite This: *J. Phys. Chem. C* 2020, 124, 6454–6460

Read Online

ACCESS |



Metrics & More

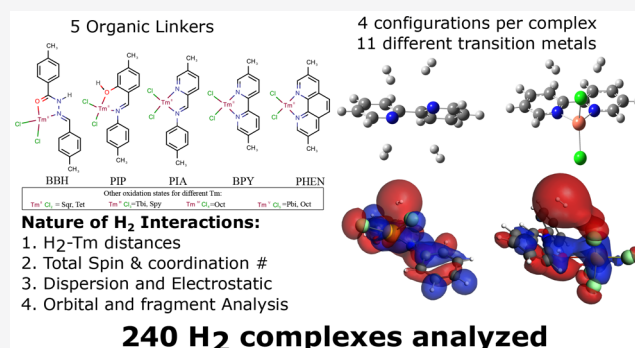


Article Recommendations



Supporting Information

ABSTRACT: The storage of hydrogen (H_2) is of economic and ecological relevance, because it could potentially replace petroleum-based fuels. However, H_2 storage at mild condition remains one of the bottlenecks for its widespread usage. In order to devise successful H_2 storage strategies, there is a need for a fundamental understanding of the weak and elusive hydrogen interactions at the quantum mechanical level. One of the most promising strategies for storage at mild pressure and temperature is physisorption. Porous materials are specially effective at physisorption, however the process at the quantum level has been under-studied. Here, we present quantum calculations to study the interaction of H_2 with building units of porous materials. We report 240 H_2 complexes made of different transition metal (Tm) atoms, chelating ligands, spins, oxidation states, and geometrical configurations. We found that both the dispersion and electrostatics interactions are the major contributors to the interaction energy between H_2 and the transition metal complexes. The binding energy for some of these complexes is in the range of at least 10 kJ/mol for many interactions sites, which is one of these main requirements for practical H_2 storage. Thus, these results are of a fundamental nature for practical H_2 storage in porous materials.



1. INTRODUCTION

The world's increasing energy demands, limited petroleum feed stocks, and increasing greenhouse gas emissions are forcing us to restructure our energy economy toward sustainable and renewable energy sources. Finding low cost, safe, and efficient energy storage materials is a major milestone toward developing renewable energy technology which can potentially replace the carbon-based fossil fuels. In this context, molecular hydrogen, or H_2 for short, with an energy content of 142 MJ kg^{-1} is an ideal and widely accepted green fuel because of its environmental friendliness, and sustainability. H_2 has an energy density much greater than gasoline and emits no greenhouse gases such as carbon dioxide (CO_2) or carbon monoxide (CO) after burning. One of the biggest challenges to reach practical applications is to achieve high density hydrogen storage at mild conditions. Free hydrogen does not occur naturally in large quantities, and it should be generated from some other renewable energy sources, e.g., artificial photosynthesis.¹ In other words, H_2 is an energy carrier (like electricity), not a primary energy source (like coal). For the advancement of hydrogen technologies to be used in transportation and other many applications; the research on hydrogen production, storage, and transformation should be further developed. Thus, hydrogen storage is a key enabling technology. Accordingly, an energy efficient method for the storage of H_2 is a necessary technology for its effective use as a fuel.

Recently, several studies and investigations showed that the addition of a transition metal (Tm) atom inside porous materials increases the total capacity of H_2 storage.^{2–5} A reversible mechanism for adsorption and release of H_2 at mild conditions is needed for any practical storage application, which can be achieved with physisorption. Some examples of storage materials capable of physisorption are metal–organic frameworks (MOFs), covalent organic frameworks (COFs), and zeolites, to mention a few.^{2–6} It has been hypothesized that the ideal range for the heat of adsorption (Q_{st}) is around 7–15 kJ/mol for efficient charge/discharge physisorption at ambient temperature (233–258 K).⁶ Recent work has shown that the Q_{st} can be approximated by the binding enthalpy (ΔH_{bind}^0) computed by first-principles calculations.² However, the nature of the interactions of the porous materials' molecular components with H_2 has not been studied in detail. Accordingly, we present a study of these interactions. Current materials reach heats of adsorption of less than 8 kJ/mol and decay as the first sorption sites are saturated at ambient temperature.^{7,8} At the

Received: December 26, 2019

Revised: February 20, 2020

Published: February 21, 2020



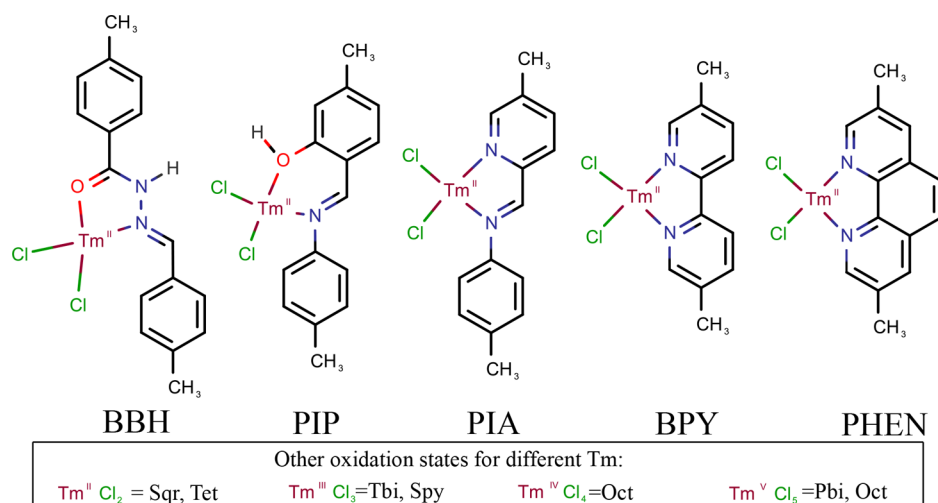


Figure 1. Different kinds of Ligands ((*E*)-*N'*-benzylidene-benzohydrazide (**BBH**), (*E*)-2-((phenylimino) methyl) phenol (**PIP**), (*E*)-*N*-(pyridin-2-ylmethylene) aniline (**PIA**), 2,2'-bipyridine (**BPY**), and phenanthroline (**PHEN**)) used as linkers in the design of crystalline porous materials which contain plausible transition metal binding sites. Notice the change of geometry for different oxidation states.

fundamental level, H_2 can interact with other atoms, molecules, and solids via electrostatics, dispersion, and orbital interactions.^{9–11} The initial studies made use mostly of dispersion interactions which are weak, while the orbital interactions are the strongest. However, the nature of H_2 interaction with *d* orbitals of the chelated Tm atoms inside a nanoporous is not well established yet.

In this article, the fundamental origin of the H_2 interactions with chelated transition metals is explained based on first-principles calculations.^{12–14} Thus, we used unrestricted B3LYP-D3 level of theory that takes into account dispersion and orbital interactions of the Tm.^{15–21} The detailed computational methods are described in the [Supporting Information](#), and a short description has been provided in the method section. The primary goal of this paper is to present a fundamental investigation into the interaction between hydrogen and organic linkers to understand the chemical principles which influence the overall adsorption and storage, which can be used in COFs, MOFs, or other porous materials. Crystalline porous materials such as MOFs and COFs are linked by organic ligands (also known as “linker”), which can integrate organic units with atomic precision into periodic structures.^{2,5,18} The linkers studied here are shown in [Figure 1](#): (*E*)-*N'*-benzylidene-benzohydrazide (**BBH**), (*E*)-2-((phenylimino) methyl) phenol (**PIP**), (*E*)-*N*-(pyridin-2-ylmethylene) aniline (**PIA**), 2,2'-bipyridine (**BPY**),^{22,23} and phenanthroline (**PHEN**). These linkers have been chosen because they are reported experimentally and some of these linkers have been used for some COFs and MOFs already.² We studied all of the expected geometries: square planar (Sqr), tetrahedral (Tet), trigonal bipyramidal (Tbi), square pyramidal (Spy), octahedral (Oct), and pentagonal bipyramidal (Pbi). We investigated the most common oxidation state of the Tm atoms which are noted in parentheses: Sc(III), V(V), Ti(IV), Cr(III), Mn(II), Fe(II), Co(II), Ni(II), Cu(II), and precious transition metals: Pd(II) and Pt(II). Different spins states configurations were calculated for each Tm complex (see the [SI](#)). If these compounds and interactions are understood well, then the design principles for H_2 storage materials will follow. We expect that this study will be able to provide some guidelines for the preparation of future

successful H_2 adsorbing linkers, which will offer more H_2 storage.

2. METHODS

First-principles calculations based on hybrid density functional theory (DFT, here B3LYP) with the localized Gaussian type basis sets were used to perform all computations as implemented in the Amsterdam Density Functional (ADF) suite code.^{24–26} The unrestricted B3LYP hybrid functional was used with Grimme's (-D3) dispersion corrections parameters, i.e., UB3LYP-D3.^{1,5,12–17,21,27,28} To incorporate the long-range dispersion effects in the present computations, Grimme's dispersion corrections parameters have added in the DFT method which is essential for the weakly bound systems.^{1,5,15–17,21,27,28} The correlation consistent triple- ζ quality basis sets (cc-pVTZ) of all atoms were used to perform all of the calculations, including obtaining the equilibrium geometry. Radial and angular points of the integration grid were generated through Gauss-Legendre radial quadrature and Lebedev two-dimensional angular point distributions. Vibrational frequencies of the adsorbates were calculated for the optimized structures in order to obtain the equilibrium geometry. The unrestricted DFT approach was used to consider the spin polarization in the present calculations. The detail description of computational methods can be found in the [Supporting Information](#).

3. RESULTS AND DISCUSSIONS

The 1st studied parameter is the distance of chelated Tm to the centroid of the first adsorbed H_2 molecule as shown in [Figure 2a](#) (top). In pristine ligands, without any Tm, the distances are measured to the centroid of the binding site of the Tm, i.e., between O–N or N–N. Our calculations showed that Cr(III) has the shortest distance between the Tm and the pristine ligands, which suggest that the interaction is among the strongest of all of the first row Tm atoms. The distance between the H_2 molecule and any particular Tm varies only slightly with the type of ligand. However, the magnitude of the binding enthalpy increases as the distance between Tm and H_2 decreases as shown in [Figure 2a](#) (bottom). In the case of **PIP** ([Figure 2a](#)), the binding sites contain –OH where the H atom may rotate. This H atom rotation may explain the higher variation in binding

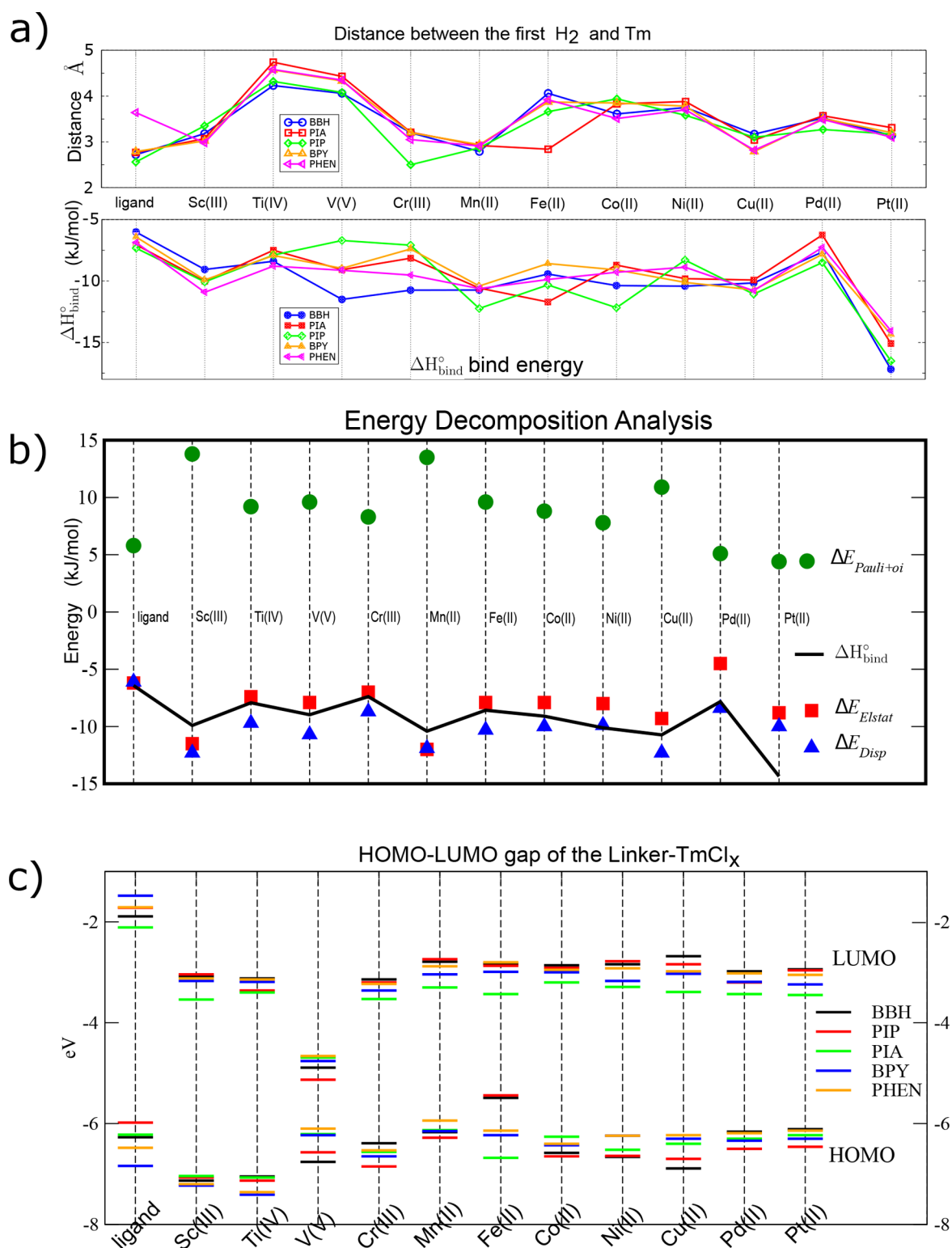


Figure 2. (a) Distance between chelated Tm with linkers (BBH, PIA, PIP, BPY, and PHEN) to the first H₂ molecule (top) and the binding energy (bottom); (b) their energy decomposition analysis; and (c) HOMO–LUMO gap.

enthalpy observed in PIP compared to other ligands. We found that the linkers chelated with Pt(II) have the most negative value of H₂ binding enthalpy, $\Delta H_{\text{bind}}^{\circ}$, which indicates they form the most stable complexes among all chelated compounds studied here. The average value of the binding energy for these Tm complexes is very close to the desired ideal $\Delta H_{\text{bind}}^{\circ}$ for reversible physisorption of 7–15 kJ/mol. Thus, our present study

demonstrates that the linkers chelated with Tm will bind H₂ more strongly. The linkers discussed are based on widely used chelating groups in coordination chemistry and can be used as building blocks for future porous materials. Energy decomposition analysis (EDA) and HOMO–LUMO gap of all of the systems studied here are computed at the same level of theory, i.e., B3LYP-D3 and shown in Figure 2b,c.

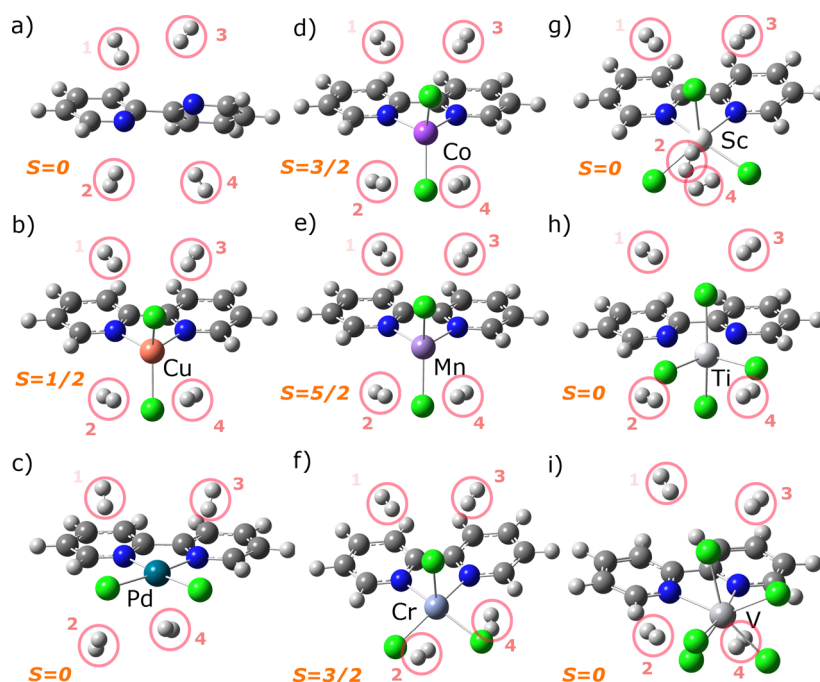


Figure 3. Configurations **BPY-TmCl_x** complexes interacting with the first 4 H₂ are shown: (a) ligand alone; (b) **BPY-CuCl₂**, Cu(II) with $S = 1/2$; (c) **BPY-PdCl₂**, Pd(II) with $S = 0$; (d) **BPY-CoCl₂**, Co(II) with $S = 3/2$; (e) **BPY-MnCl₂**, Mn(II) with $S = 5/2$; (f) **BPY-CrCl₃**, Cr(III) with $S = 3/2$ forms a square pyramidal geometry; (g) **BPY-ScCl₃**, Sc(III) with $S = 0$ forms a trigonal bipyramidal; (h) **BPY-TiCl₄**, Ti(IV) with $S = 0$ has octahedral geometry; and (i) **BPY-VCl₅**, V(V) with $S = 0$ forms a pentagonal bipyramidal geometry.

The 2nd studied parameter is the geometry which depends on the total spin number S and coordination number.^{29,30} The optimized structures of the chelated, **BPY**, interacting with four H₂ molecules are shown in Figure 3. The numbers next to the H₂ molecules represent the sequence of the H₂ addition to the **BPY-TmCl_x**. We choose **BPY** for the configuration analysis because **BPY** is highly symmetric; therefore, the local minima sites for the H₂ are unrelated to other parameters such as dihedral angle of the linker-TmCl_x complex. For the ligand alone, the H₂ molecules form symmetrical configurations relative to the binding site (Figure 3a). The chelated **BPY-TmCl_x** complexes (where Tm = Cu, Pd, Co, Mn, Cr, Sc, Ti, and V) interacting with various H₂ molecules are shown in Figure 3b–i.

In the chelated-Tm with the square geometry: Cu(II), Pd(II), and Pt(II), the first two H₂ molecules are located at the open sites of the Tm, which are above and below the Tm (as shown in Figure 3b,c except Pt(II)), while the third H₂ displaces the first H₂ from its initial location. Stronger binding enthalpy is observed for any Tm, in the tetrahedral geometry than in the square planar geometry. For example, in the **BBH-NiCl₂** complex, the Ni(II) has spin $S = 2/2$ in the tetrahedral geometry with a binding enthalpy of 1.2 kJ/mol more negative than the square planar geometry with spin $S = 0$. On the other hand, **PIP-CoCl₂** with spin $S = 3/2$ and $S = 1/2$ are in a tetrahedral geometry and have H₂ similar binding enthalpies with less than 0.1 kJ/mol difference. Only the Tm with $S = 0$ can have a perfect square geometry, e.g., Cu(II) with $S = 1/2$ forms a distorted square geometry compound. In Co(II), Fe(II), Mn(II), and Ni(II) with the tetrahedral geometry the first two H₂ molecules are on top or bottom of the ligand-TmCl_x complex and weakly polarized toward the Cl[−] ions (Figure 3d of the **BPY-CoCl₂**). With the addition of the third and fourth H₂ molecules, the location of H₂ molecules rearrange mostly into typical configurations (Figure 3e–i). Transition metals with higher

oxidation states: Cr(III), Sc(III), V(V), and Ti(IV) form square pyramidal, trigonal bipyramidal, octahedral, or pentagonal bipyramidal geometries, respectively. The first H₂ molecule has a minimum energy at the nearest possible location to the Tm and binding sites (N or O atoms). Some Tm have different geometries depending on the bond length and ligand such as in the ligand-VCl₅ complexes. V(V) has pentagonal bipyramidal geometry in **PIA**, **BPY**, and **PHEN** while octahedral geometry in **BBH** and **PIP**. In general, the distance between H₂ to the Tm in the pentagonal bipyramidal (Pbi) and octahedral (Oct) geometries are about 1 Å longer than other geometries because of the smaller amount of available space for the H₂ to interact directly with the Tm, and consequently have lower binding enthalpy. In the trigonal bipyramidal Sc(III) and square pyramidal Cr(III) configurations, the binding enthalpies are comparable to the square planar and tetrahedral geometries, respectively. In the case of Sc(III) or Cr(III), the first H₂ have strong binding enthalpy because it can get close (~ 2.8 Å) to the Tm centers and thus more interactions occur.

The 3rd studied parameter is the effect of electrostatics and dispersion interactions between the H₂ molecules and the linker-TmCl_x complexes. The leading permanent multipole moment of the H₂ is a weak quadrupole moment, but it could also have weak induced dipole moment.^{9,10,31} A fragment analysis proposed by Ziegler and Berends has been performed to decompose the binding enthalpy.^{32,33} To illustrate this we showed two cases: the H₂ with a quadrupole moment is attracted to Cu(II) more than to V(V) by about 2.8 kJ/mol. In all of these compounds, the effect of electrostatics is 5% smaller than the dispersion. The dispersion energy, electrostatics, Pauli repulsions, and orbital interactions in the binding enthalpy between the Tm-ligand complexes and H₂ for **BPY** are shown in Figure 2b. This analysis shows that the dispersion energy and electrostatics are the dominant factors for the magnitude of the binding enthalpy. The

other ligands follow a similar trend as BPY (Supporting Information, section 2).

The 4th studied parameter is the possible orbital interactions between the s orbitals of H_2 and the d orbitals of the Tm. This can be estimated by the occupied molecular orbitals (MO) of the complexes shown in Figure 4. In Figure 4b the occupied MO

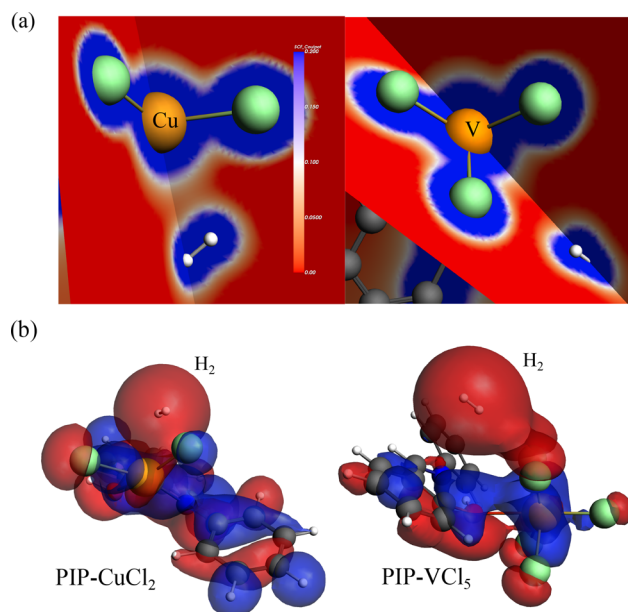


Figure 4. HOMO–LUMO orbitals projected in (a) planes and (b) space for $PIP-CuCl_2+H_2$ and $PIP-VCl_5+H_2$ complexes. In the former the H_2 interacts mostly with $Cu(II)$, while in the later, the H_2 interacts more with Cl^- than with the $V(V)$ atom.

has some overlap between the s orbital from H_2 and d orbital of $Cu(II)$. A similar phenomenon is observed in the $PIP-VCl_5$ complex. The orbital interaction depends on the overlap between the interacting orbitals and decays exponentially with the distance between H_2 and ligand– $TmCl_x$ complex.⁹

Fragment analysis has been performed to differentiate the molecular orbitals (MO) from each components of the complex (H_2 , linker, and $TmCl_x$). The fragment analysis also computes the contributing components of total energy. The s orbitals of H_2 molecules are overlapped with the d orbitals of Tm atoms in the linker– $TmCl_x$ complexes, e.g., about 70% contribution of molecular orbitals from H_2 s orbitals are overlapped with the d orbitals of the Cu atom in the $PIP-CuCl_2$ complex (Figure 4). Typically, the energy level of the occupied MO (HOMO) of H_2 molecule alone (-11.72 eV) is far below the HOMO (-6.72 eV) of the whole system, e.g., $CuCl_2-PIP + H_2$ as shown in Figure 5. This is consistent with the H_2 as a poor charge donor because of the deep energy level of its σ bonding of -11.72 eV and also a poor charge acceptor because of the high level of its σ^* antibonding (beyond the scale of Figure 5). The profiles of HOMO and LUMO gap of all of the complexes is shown in Figure 2c. The HOMO–LUMO energy gap of the pure ligand is higher than any chelated complex. The ligand– VCl_5 complexes have the lowest gap at ~ 1.2 eV. Most of the complexes have an energy gap in the visible light spectrum (1.6 – 3.2 eV); therefore, these complexes are promising candidates as dye sensitizers. Uptakes in weight percentage (% wt) for H_2 in the linkers and linker–metal complexes have been estimated. They fall in the range of 1.62 – 4.92 % wt, which is similar to COFs with similar linkers (see Table S6 in the Supporting Information). This is

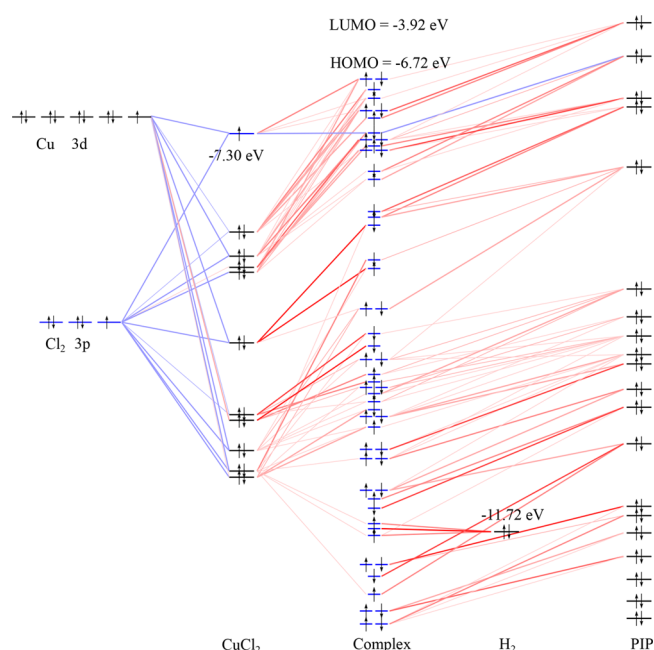


Figure 5. Molecular orbitals (MO) of the complex with linker– $CuCl_2$ and one H_2 . The components of the complex are decomposed as Cu, Cl_2 , $CuCl_2$, and linker PIP . The MO at the level of ~ -11.72 eV are composed mainly from the s orbitals of H_2 and some contribution from the d -orbital of transition metal $Cu(II)$.

another consequence of the relationship between binding energy (ΔH_{bind}) and the heat of adsorption (Q_{st}).

4. CONCLUSIONS

In summary, the nature of intermolecular interactions between H_2 and linker– $TmCl_x$ complexes is presented. The favorable sites for the H_2 molecules interactions depend mainly on the type of the Tm, spin, and available space. An important conclusion of this work concerns the design of chelated linkers for crystalline porous materials such as COFs and MOFs. The chelation of Tm inside porous frameworks through their linkers can enhance the effective H_2 storage as the interaction between the Tm atoms and H_2 can be tuned to get higher binding enthalpy ΔH_{bind}° . Ultimately, the ability of the chelated linkers to bind H_2 molecules is highly dependent on the Tm coordination sphere, with the most important interaction given by the dispersion and electrostatics.

■ ASSOCIATED CONTENT

Supporting Information

The Supporting Information is available free of charge at <https://pubs.acs.org/doi/10.1021/acs.jpcc.9b11939>.

Computational details and chelated complexes with the H_2 optimized linker structures and their descriptions; H_2 uptakes in terms of weight percentage (% wt) of both the pristine linkers and linker–metal complexes; and optimized geometries of the chelated complexes with H_2 (PDF)

■ AUTHOR INFORMATION

Corresponding Authors

Srimanta Pakhira – Discipline of Physics and Discipline of Metallurgy Engineering and Materials Science, Indian Institute of Technology Indore, Indore 453552, Madhya Pradesh, India;

orcid.org/0000-0002-2488-300X; Email: spakhira@iiti.ac.in

Jose L. Mendoza-Cortes — Department of Chemical & Biomedical Engineering, Florida A&M University—Florida State University (FAMU-FSU) College of Engineering, Tallahassee, Florida 32310, United States; Condensed Matter Theory, National High Magnetic Field Laboratory (NHMFL), Department of Scientific Computing, Materials Science and Engineering, High Performance Materials Institute, and Department of Physics, Florida State University, Tallahassee, Florida 32310, United States; orcid.org/0000-0001-5184-1406; Phone: +1-850-410-6298; Email: mendoza@eng.famu.fsu.edu; Fax: +1-850-410-6150

Complete contact information is available at:
<https://pubs.acs.org/10.1021/acs.jpcc.9b11939>

Notes

The authors declare no competing financial interest.

ACKNOWLEDGMENTS

J.L.M.-C. was supported by Florida State University (FSU). The authors gratefully acknowledge the support from the Energy and Materials Initiative and the High Performance Material Institute (HPMI) facilities at FSU. S.P. thanks the Science and Engineering Research Board-Department of Science and Technology (SERB-DST), Government of India for providing the Ramanujan Faculty Fellowship under the Grant No. SB/S2/RJN-067/2017. A portion of this work was performed at the National High Magnetic Field Laboratory, which is supported by National Science Foundation Cooperative Agreement No. DMR-1644779 and the State of Florida. The authors thank the High Performance Computer cluster at the Research Computing Center (RCC) at FSU for providing computational resources and support.

REFERENCES

- (1) Lucht, K. P.; Mendoza-Cortes, J. L. Birnessite: A Layered Manganese Oxide To Capture Sunlight for Water-Splitting Catalysis. *J. Phys. Chem. C* **2015**, *119*, 22838–22846.
- (2) Pramudya, Y.; Mendoza-Cortes, J. L. Design Principles for High H₂ Storage Using Chelation of Abundant Transition Metals in Covalent Organic Frameworks for 0–700 bar at 298 K. *J. Am. Chem. Soc.* **2016**, *138*, 15204–15213.
- (3) Yildirim, T.; Hartman, M. R. Direct Observation of Hydrogen Adsorption Sites and Nanocage Formation in Metal–Organic Frameworks. *Phys. Rev. Lett.* **2005**, *95*, 215504.
- (4) Arter, C. A.; Zuluaga, S.; Harrison, D.; Welchman, E.; Thonhauser, T. Fivefold Increase of Hydrogen Uptake in MOF–74 Through Linker Decorations. *Phys. Rev. B: Condens. Matter Mater. Phys.* **2016**, *94*, 144105.
- (5) Pakhira, S.; Mendoza-Cortes, J. L. Intercalation of First Row Transition Metals Inside Covalent–Organic Frameworks (COFs): A Strategy to Fine Tune the Electronic Properties of Porous Crystalline Materials. *Phys. Chem. Chem. Phys.* **2019**, *21*, 8785–8796.
- (6) Aduenko, A. A.; Murray, A.; Mendoza-Cortes, J. L. General Theory of Absorption in Porous Materials: Restricted Multilayer Theory. *ACS Appl. Mater. Interfaces* **2018**, *10*, 13244–13251.
- (7) Han, S. S.; Goddard, W. A. Lithium-doped Metal–Organic Frameworks for Reversible H₂-Storage at Ambient Temperature. *J. Am. Chem. Soc.* **2007**, *129*, 8422–8423.
- (8) Bhatia, S. K.; Myers, A. L. Optimum Conditions for Adsorptive Storage. *Langmuir* **2006**, *22*, 1688–1700.
- (9) Lochan, R. C.; Head-Gordon, M. Computational Studies of Molecular Hydrogen Binding Affinities: The Role of Dispersion Forces, Electrostatics, and Orbital Interactions. *Phys. Chem. Chem. Phys.* **2006**, *8*, 1357–1370.
- (10) Pascal, T. A.; Boxe, C.; Goddard, W. A. An Inexpensive, Widely Available Material for 4 wt % Reversible Hydrogen Storage Near Room Temperature. *J. Phys. Chem. Lett.* **2011**, *2*, 1417–1420.
- (11) Kubas, G. J. Fundamentals of H₂ Binding and Reactivity on Transition Metals Underlying Hydrogenase Function and H₂ Production and Storage. *Chem. Rev.* **2007**, *107*, 4152–4205.
- (12) Becke, A. D. Density-Functional Exchange-energy Approximation with Correct Asymptotic Behavior. *Phys. Rev. A: At., Mol., Opt. Phys.* **1988**, *38*, 3098–3100.
- (13) Becke, A. D. Density-Functional Thermochemistry. III. The Role of Exact Exchange. *J. Chem. Phys.* **1993**, *98*, 5648–5652.
- (14) Lee, C.; Yang, W.; Parr, R. G. Development of the Colle-Salvetti Correlation-Energy Formula into a Functional of the Electron Density. *Phys. Rev. B: Condens. Matter Mater. Phys.* **1988**, *37*, 785–789.
- (15) Grimme, S. Semiempirical GGA-type Density Functional Constructed with a Long-range Dispersion Correction. *J. Comput. Chem.* **2006**, *27*, 1787–1799.
- (16) Grimme, S.; Antony, J.; Ehrlich, S.; Krieg, H. A Consistent and Accurate Ab Initio Parametrization of Density Functional Dispersion Correction (DFT-D) for the 94 Elements H–Pu. *J. Chem. Phys.* **2010**, *132*, 154104.
- (17) Pakhira, S.; Mendoza-Cortes, J. L. Tuning Dirac Cone of Two Dimensional Bilayer Graphene and Graphite by Intercalating First Row Transition Metals using First Principles. *J. Phys. Chem. C* **2018**, *122*, 4768–4782.
- (18) Pakhira, S.; Lucht, K. P.; Mendoza-Cortes, J. L. Iron Intercalated Covalent–Organic Frameworks: A Promising Approach for Semiconductors. *J. Phys. Chem. C* **2017**, *121*, 21160–21170.
- (19) Hui, J.; Pakhira, S.; Bhargava, R.; Barton, Z. J.; Zhou, X.; Chinderle, A. J.; Mendoza-Cortes, J. L.; Rodriguez-Lopez, J. Modulating Electrocatalysis on Graphene Heterostructures: Physically Impermeable Yet Electronically Transparent Electrodes. *ACS Nano* **2018**, *12*, 2980–2990.
- (20) Niu, W.; Pakhira, S.; Marcus, K.; Li, Z.; Mendoza-Cortes, J. L.; Yang, Y. Apically Dominant Mechanism for Improving Catalytic Activities of N-Doped Carbon Nanotube Arrays in Rechargeable Zinc–Air Battery. *Adv. Ene. Mater.* **2018**, *8*, 1800480.
- (21) Pakhira, S.; Lucht, K. P.; Mendoza-Cortes, J. L. Dirac Cone in Two Dimensional Bilayer Graphene by Intercalation with V, Nb, and Ta Transition Metals. *J. Chem. Phys.* **2018**, *148*, 064707.
- (22) Ghosh, M.; Biswas, P.; Florke, U.; Nag, K. Halogen Exchange and Scrambling between C–X and M–X Bonds in Copper, Nickel, and Cobalt Complexes of 6,6-bis(bromo/chloromethyl)-2,2-bipyridine: Structural, Electrochemical, and Photochemical Studies. *Inorg. Chem.* **2008**, *47*, 281–296.
- (23) Wu, H.-P.; Janiak, C.; Rheinwald, G.; Lang, H. 5,5-Dicyano-2,2'-Bipyridine Silver Complexes: Discrete Units or Co-ordination Polymers through a Chelating and/or Bridging Metal–Ligand Interaction. *J. Chem. Soc., Dalton Trans.* **1999**, 183–190.
- (24) Fonseca Guerra, C.; Snijders, J. G.; Te Velde, G.; Baerends, E. J. Towards an Order-N DFT Method. *Theor. Chem. Acc.* **1998**, *99*, 391–403.
- (25) te Velde, G.; Bickelhaupt, F. M.; Baerends, E. J.; Fonseca Guerra, C.; van Gisbergen, S. J. A.; Snijders, J. G.; Ziegler, T. Chemistry with ADF. *J. Comput. Chem.* **2001**, *22*, 931–967.
- (26) Universiteit, V. ADF2016, SCM, Theoretical Chemistry, 2016; <http://www.scm.com>.
- (27) Lei, Y.; Pakhira, S.; Fujisawa, K.; Wang, X.; Iyiola, O. O.; Perea Lopez, N.; Laura Elias, A.; Pulickal Rajukumar, L.; Zhou, C.; Kabius, B.; Alem, N.; Endo, M.; Lv, R.; Mendoza-Cortes, J. L.; Terrones, M.; et al. Low-temperature Synthesis of Heterostructures of Transition Metal Dichalcogenide Alloys (W_xMo_{1-x}S₂) and Graphene with Superior Catalytic Performance for Hydrogen Evolution. *ACS Nano* **2017**, *11*, 5103–5112.
- (28) Hui, J.; Schorr, N. B.; Pakhira, S.; Qu, Z.; Mendoza-Cortes, J. L.; Rodriguez-Lopez, J. Achieving Fast and Efficient K⁺ Intercalation on

Ultrathin Graphene Electrodes Modified by a Li^+ Based Solid-Electrolyte Interphase. *J. Am. Chem. Soc.* **2018**, *140*, 13599–13603.

(29) Thonhauser, T.; Zuluaga, S.; Arter, C.; Berland, K.; Schröder, E.; Hyldgaard, P. Spin Signature of Nonlocal Correlation Binding in Metal-Organic Frameworks. *Phys. Rev. Lett.* **2015**, *115*, 136402.

(30) Sun, Y. Y.; Kim, Y.-H.; Zhang, S. B. Effect of Spin State on the Dihydrogen Binding Strength to Transition Metal Centers in Metal-Organic Frameworks. *J. Am. Chem. Soc.* **2007**, *129*, 12606–12607.

(31) Stern, A. C.; Belof, J. L.; Eddaoudi, M.; Space, B. Understanding Hydrogen Sorption in a Polar Metal-Organic Framework with Constricted Channels. *J. Chem. Phys.* **2012**, *136*, 034705.

(32) Bickelhaupt, F. M.; Baerends, E. J. *Reviews in Computational Chemistry*; John Wiley & Sons, Inc.: Hoboken, NJ, 2000; p 1.

(33) Ziegler, T.; Rauk, A. On the Calculation of Bonding Energies by the Hartree-Fock Slater Method. *Theoret. Chim. Acta* **1977**, *46*, 1–10.